Precision Engineering 35 (2011) 525–535

Contents lists available at ScienceDirect

Precision Engineering

journal homepage: www.elsevier.com/locate/precision

Technical note

Sensor design and evaluation for on-machine probing of extruded tool joints

Arthur Graziano, Tony L. Schmitz*

University of Florida, Machine Tool Research Center, Gainesville, FL 32611, United States

ARTICLE INFO

Article history:
Received 24 May 2010
Received in revised form 7 December 2010
Accepted 23 February 2011
Available online 4 March 2011

Keywords:
Extrusion
Turning
LVDT
Adaptive control

ABSTRACT

This paper describes the design and evaluation of two contact probes used to measure the length and bore concentricity of cylindrical, extruded tool joints while clamped in a production lathe spindle. The probes consisted of an LVDT, a spring-preloaded shaft supported by linear bearings used to isolate the LVDT from side loads, and a hardened steel sphere to contact the rough surface. For bore concentricity measurements, a parallelogram leaf-type flexure and 45° surface was used to transfer radial deviations to the spindle/part/LVDT axis. The LVDT output was used in conjunction with the lathe turret position to determine the extruded part dimensions prior to machining. Experimental results are provided for measurements of multiple parts; variations in length, internal diameter, and bore concentricity are compared to the nominal dimensions. Additionally, a calibration artifact is described which enabled evaluation of the measurement accuracies for the two probes. Given the pre-machining part dimensions, it is shown how this information can be used to select from a pre-defined matrix of part programs to reduce cycle time and machining cost.

1. Introduction

In the oil drilling industry, tool joints provide high-strength connections between the individual drill pipes. The axisymmetric tool joints are produced using two primary manufacturing processes: the joints are initially extruded and then finish machined. One typical obstacle to optimizing the turning performance is deviations from the nominal dimensions for the extrusions, including length variations and non-concentricity of the inner and outer diameters. This causes more or less material to be removed than commanded during the subsequent turning, boring, and facing operations. If the part is larger than nominal, a conservative machining approach is required to avoid larger depths of cut than commanded and the subsequent potential for tool/part damage and/or accelerated tool wear.

A natural alternative to conservative part paths (e.g., starting the facing operation assuming the longest possible part which can result in "cutting air" for a shorter part) is pre-machining inspection. Manual inspection (statistical sampling) is a common method for determining dimensional inaccuracies prior to machining. This can add production time and cost, however, because it typically requires that the part be transported to a separate measurement location. Additionally, statistical sampling does not ensure that all defective parts are identified unless 100% inspection is employed. One approach used to satisfy this 100% inspection requirement in a timely manner is to measure parts while they are chucked or clamped in the machine. Yandayan and Burdekin [1] provide a review of the different methods used to accomplish this task (up to 1996) and Vacharanukul and Mekid [2] continue the survey through 2003. Six measurement groups are discussed, including mechanical, optical, ultrasonic, pneumatic, electrical, and temperature detection methods.

In this study, two LVDT-based contact probes were developed to measure the length and bore concentricity of tool joints while clamped in a lathe spindle in order to provide pre-machining extrusion dimensions. The paper is organized as follows. Background information regarding the extrusion process, typical geometric deviations, and the machining platform is provided in Section 2. The sensor designs are described in Section 3. Benchtop testing results are provided in Section 4. The part measurement procedures are outlined in Section 5. Part measurement results are reported in Section 6. Conclusions are provided in Section 7.

Using the contact probes, on-machine probing can be implemented to determine the part dimensions prior to executing the part program. If the part dimensions can be identified with sufficient accuracy, the part program can be modified in real time or an alternative can be selected from a pre-defined matrix of programs based on the anticipated dimensional variations.

2. Process background

Variations in the indirect extrusion process (see Fig. 1) lead to geometric imperfections that affect the turning process. First, as the material flows up and around the pin during extrusion, a bulge can

* Corresponding author. Tel.: +1 352 392 8909; fax: +1 352 392 1071.
E-mail address: tschmitz@ufl.edu (T.L. Schmitz).

0141-6359/$ – see front matter © 2011 Elsevier Inc. All rights reserved.
doi:10.1016/j.precisioneng.2011.02.010

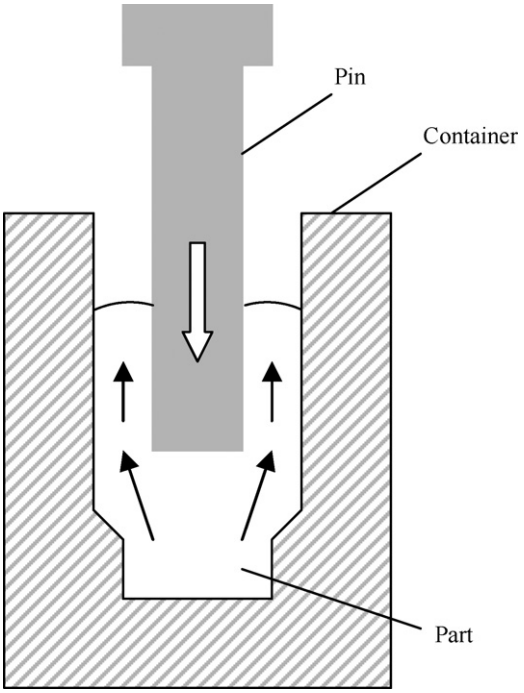

Fig. 1. Indirect extrusion process.

Fig. 2. Photograph of typical extrusion. The length is 520.7 mm and the mass is 76 kg.

be created at the end; the bulge peak is not necessarily located at the midpoint between the inner and outer diameters. Second, length variations occur due to fluctuations in the part temperature (a high-temperature shearing operation precedes the extrusion process[1]). Third, after many extrusion cycles, the pin may both: (1) begin the extrusion off-center with respect to the container centerline; and (2) lose its parallelism to the container axis during extrusion.

[1] In this paper, the process flow for a particular production facility is described. While the manufacturing details may differ in other locations, the authors believe that these conditions are sufficiently representative to warrant a discussion of this research effort.

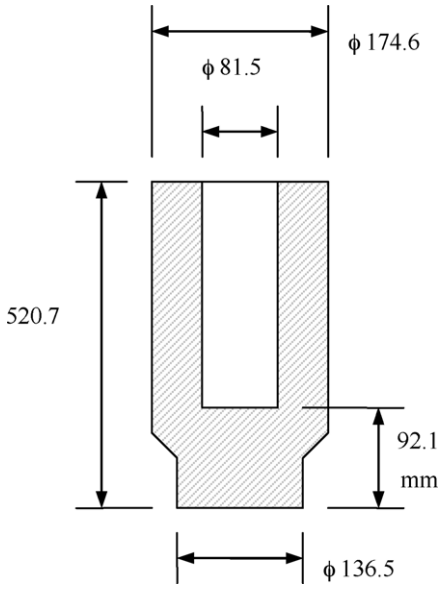

Fig. 3. Extrusion nominal dimensions.

The combination of these issues generates parts with length variation, non-flat ends, and non-concentric bores (with non-constant concentricity along the bore length).

After extrusion, the parts are allowed to cool outside before being transferred to the shop floor for the final machining process. This can result in oxidation and scale on the part surface. A photograph of a typical extrusion measured as part of this study is provided in Fig. 2; it is seen that the surface is rough with significant oxidation. The nominal dimensions for the 76 kg steel part are given in Fig. 3. Specified variation in the extrusion length is +6.4/−0 mm, while variation in the bore diameter is +0/−1.5 mm.

The extruded parts are machined on Okuma LC-40 lathes, which include two independent turrets. The upper turret (A) is used to perform boring and drilling operations on the extrusions, while the lower turret (B) is used for facing and turning cuts. The turrets enable relative motion between the part and tool in both the z (parallel to the spindle centerline) and x (diametral) directions. The LC-40 lathe can accommodate a maximum part diameter of 400 mm with a working

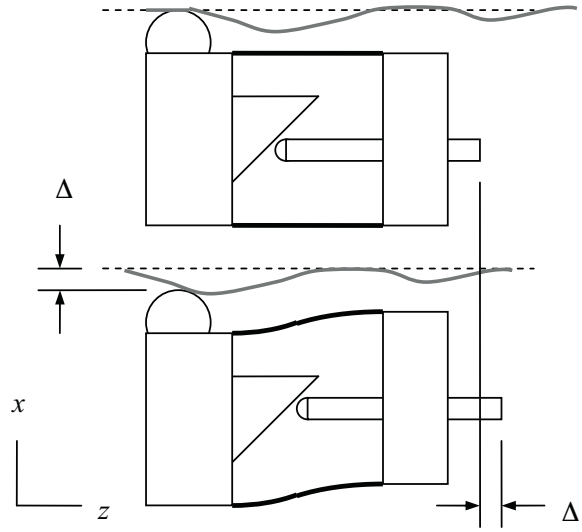

Fig. 4. One-to-one ratio between x direction surface location and z direction shaft motion.

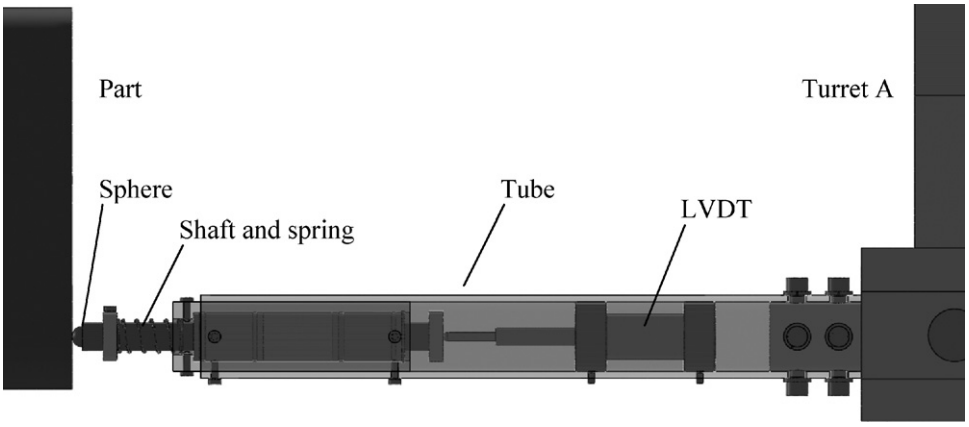

Fig. 5. Length probe solid model.

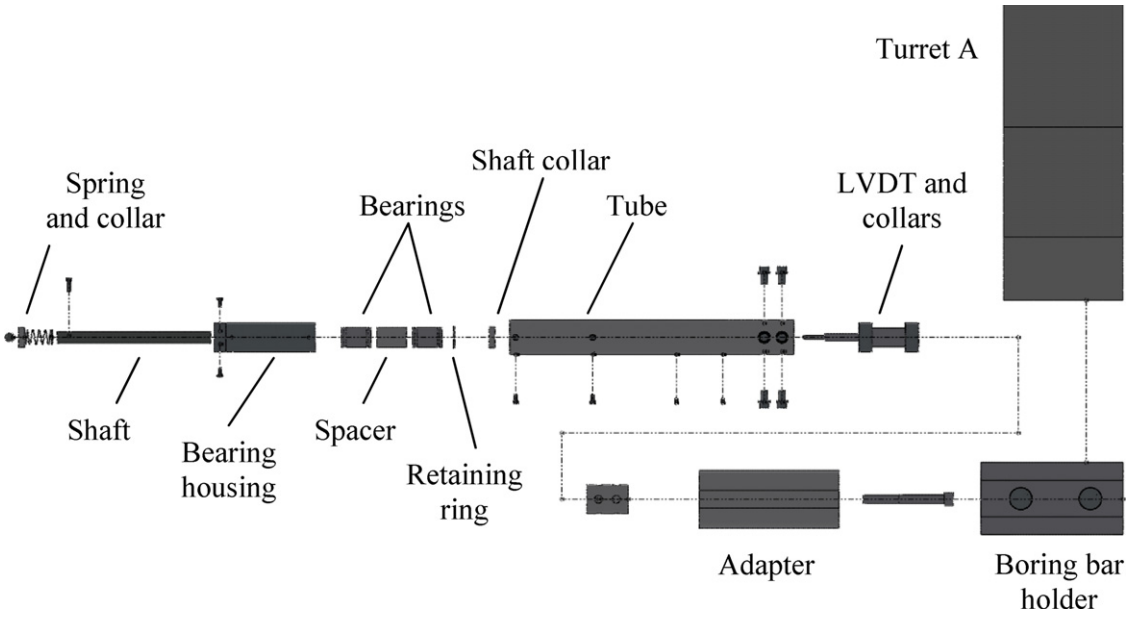

Fig. 6. Exploded view of length probe.

length of 750 mm. The spindle is rated for 37 kW of continuous power.

3. Sensor design

In order to perform the pre-machining measurements, a linear variable differential transformer (LVDT)-based design was chosen for the contact probes. LVDTs consist of a transformer and an iron core armature that slides through the transformer. The transformer is composed of three coils: a center primary coil with secondary coils on either side. As current is supplied to the primary coil, a voltage is induced in the secondary coils that is linearly proportional to the position of the sliding core [3]. The LVDT chosen for this application was the RDP Electrosense DCTH300AG transducer

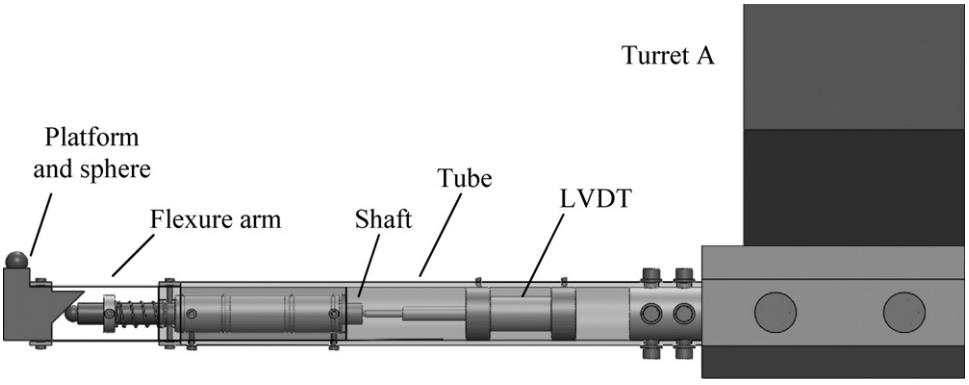

Fig. 7. Concentricity probe solid model.

[4]. This model was selected because it includes built-in electronics that enable a DC supply and output and its range of ±7.5 mm was adequate.

Three measurements were required to define the part geometry: length, inside diameter, and bore concentricity (the outer diameter was considered to be sufficiently accurate based on prior experience). The length measurement could be completed by contacting the extrusion face in the z direction. However, the latter two measurements required contact with the (inner) bore diameter. Because it was inconvenient to align the LVDT axis in the x direction within the bore (based on LVDT sizes and the bore diameter), a design was required that would transfer motion along the surface normal of the inside diameter to the z direction, where it was convenient to orient the LVDT axis. A parallelogram leaf-type flexure and 45° surface were chosen to accomplish this task. Fig. 4 demonstrates the design concept, where x displacement of the platform caused by variation in the surface location is transferred to the z direction via the 45° surface (nominally a one-to-one ratio).

The depths of cut for roughing passes are up to 5.1 mm. A 1% error in the commanded depth of cut is therefore 51 μm. Assuming that this 1% error is an acceptable variation in the actual depth of cut, the target uncertainty for the two probes was set to 50 μm.

3.1. Length probe

It was determined that side (lateral) loading of the LVDT resulted in poor transducer performance. Therefore, a shaft supported by linear ball bearings was incorporated to resist the inherent side loading from the rough extrusion surface and transfer only axial motion to the LVDT. Fig. 5 shows the design, where the 12.7 mm diameter shaft (AISI 1566 Rockwell C60) is constrained using two linear ball bearings (to increase lateral stiffness) and the LVDT is supported by two collars inside a 2024 aluminum tube (310.4 mm length). This ensures that both the shaft and LVDT share (nominally) the same motion axis. A 440C stainless steel 9.5 mm diameter sphere (grade 24, Rockwell C58-C65) is fixed to the end of the shaft; this sphere serves as the contact surface during measurements. The shaft is spring-preloaded against the part during measurements (see the collar and 720 N/m spring at the left end of the assembly in Fig. 5). The LVDT is preloaded against the shaft using its own internal spring. An exploded view is provided in Fig. 6. As shown in the figure, the probe is mounted in turret A using a boring bar holder. This ensures that the probe axis is (nominally) coincident with the z axis with a zero offset in the x direction.

3.2. Concentricity probe

Fig. 7 shows the concentricity probe design. As noted previously, this design includes a flexure and 45° surface to transfer the x direction bore surface location to the z direction (and the LVDT axis). The flexure platform carries a 12.7 mm diameter 440C stainless steel sphere (grade 100, Rockwell C58-C65) to provide contact with the bore surface. As the part rotates, the radial variation in the surface location causes the platform to be deflected in the x direction. This motion is transferred to the z axis through the 45° machined surface on the platform.[2] A shaft supported by linear bearings is again used to isolate the LVDT from side loads. A second sphere (9.5 mm diameter, grade 24, Rockwell C58-C65) is attached to the shaft which maintains contact with the 45° surface; preload is supplied by a spring/collar. To reduce friction and abrasion at the 45° surface, a thin glass sheet was epoxied to the 45° surface.

[2] An estimate of the parasitic motion (z deflection of the platform during its x translation) is provided in Appendix A.

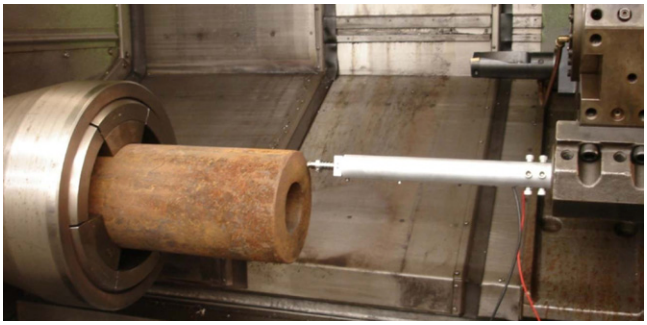

Fig. 8. Photograph of length probe on Okuma LC-40 lathe.

Photographs of the completed sensors are provided in Figs. 8 and 9. In both cases, the LVDT voltages were recorded using National Instrument data acquisition hardware and LabVIEW software.

4. Initial sensor testing

4.1. Benchtop tests

Benchtop tests were performed to verify the probe performance prior to completing part measurements on the lathe. For these initial tests, a single-axis micrometer stage was used to apply the commanded displacement, which was subsequently compared to the sensor displacement. A first activity was to establish the noise floor for the probes. Measurements using both probes in numerous setups yielded noise levels from ±14 mV to ±23 mV. This noise floor was considered acceptable given the manufacturer's maximum range of ±25 mV. Due to the presence of noise, time-average voltage values were used to calculate displacements when possible.

The length probe was tested by commanding displacements up to 2 mm in increments of 0.5 mm (both forward and reverse directions) and recording the LVDT voltage. Using the manufacturer's calibration constant of 0.65028 V/mm, the results between the stage and probe displacements agreed to within 2 μm over all tests. Based on the manufacturer's calibration uncertainty of 4.2 μm, these results were considered acceptable. Probe hysteresis was evaluated by commanding a displacement sequence of {0, 1, 3, 1, 0, 3, 1, 3, 0} mm. No significant hysteresis was observed; a maximum difference of 2 μm between the forward and reverse motions was obtained. It was noted, however, that the length probe displacements were consistently smaller than the commanded values, which suggests an instrument bias. Section 4.2 describes sensor misalignments (cosine error for the length probe) that could yield this bias.

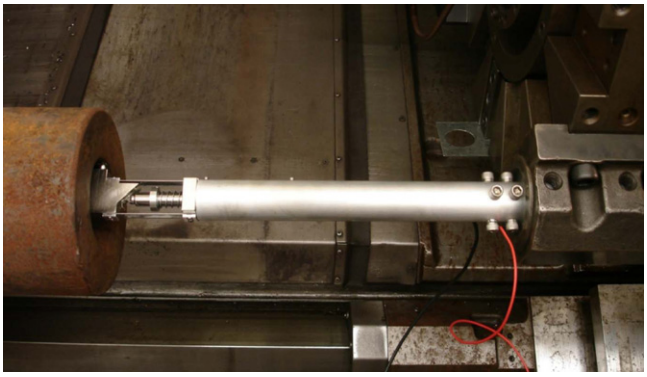

Fig. 9. Photograph of concentricity probe on Okuma LC-40 lathe.

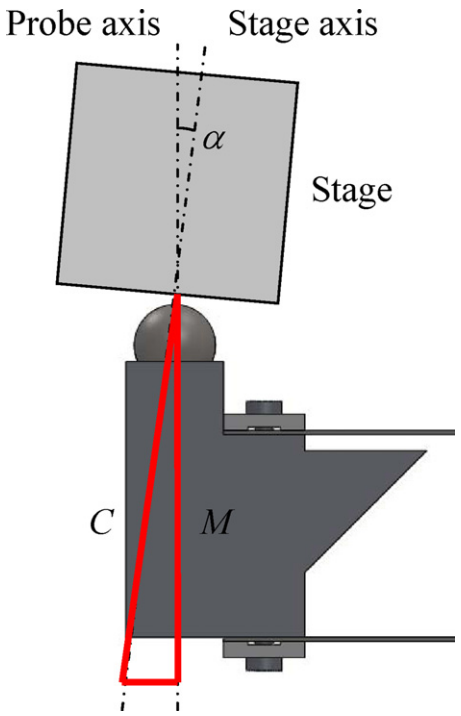

Fig. 10. Axes misalignment.

For the concentricity probe, the 0–2 mm forward and reverse tests (0.5 mm increments) were again completed. However, significant disagreement was obtained when using the manufacturer's LVDT calibration constant of 0.65153 V/mm. The probe displacements were smaller with increasing disagreement for larger commanded displacements. This bias was attributed to assembly misalignment; see Section 4.2. Because the probe measurements were repeatable, however, it was decided that the misalignments could be compensated using a least squares best fit to the measurement data to identify a new calibration constant. It was also observed that hysteresis was present in the probe assembly. It is believed that this was due to a combination of non-zero friction at the LVDT sphere/45° surface interface and finite lateral stiffness of the LVDT and linear bearings. For a stage displacement range of 3 mm (two times the diametral tolerance), the hysteresis values were 50 μm or less. While this value would be considered large for typical displacement transducers, it was within the target uncertainty for this application.

4.2. Concentricity probe misalignments

As noted, it is believed that a primary source of disagreement between the commanded (C) and measured (M) displacements was due to probe assembly and setup misalignments. Based on all benchtop tests for the concentricity probe, the average ratio of M to C was 0.989. The length probe's ratio, on the other hand, was 0.999. Therefore, the following misalignment descriptions focus on the concentricity probe.

4.2.1. Axes misalignments

Angular misalignment between the stage and probe axes leads to the familiar cosine error. As shown in Fig. 10, if the angle α was zero, then M would be equal to C in the absence of other misalignments. For the average M to C ratio of 0.989, α would have to be 8.5° to fully account for the bias observed in the benchtop tests.

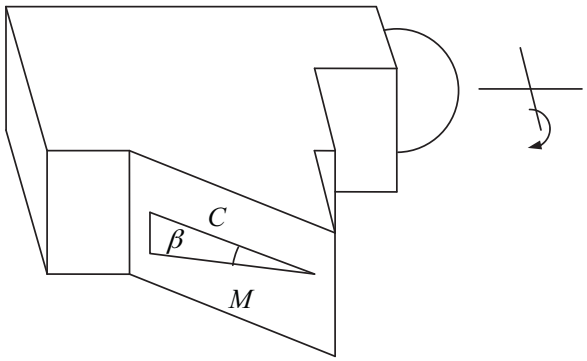

Fig. 11. Platform rotational misalignment.

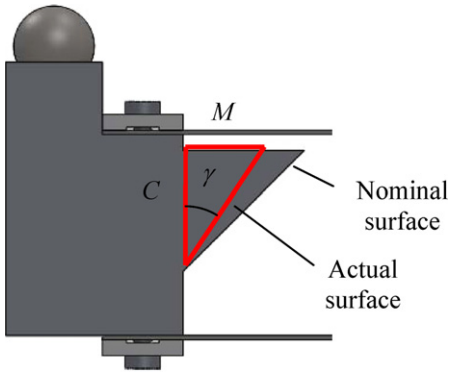

Fig. 12. 45° surface angle error.

4.2.2. Platform errors

A cosine error is caused by the angular misalignment between the flexure motion direction (defined by the flexure arms) and the platform shown in Fig. 11. Again, M would be less than C and the misalignment angle, β, would have to be 8.5° to fully account for the 0.989 M to C ratio from the benchtop tests.

An error in the angle for the 45° surface leads to a tangent error; see Fig. 12. The measured displacement is much more sensitive to this angular error. An angle that deviates by only −0.32° from 45° would account for the 0.989 M to C ratio. This angular error could be imposed by a fabrication error for the 45° surface, a misalignment of the holes use to locate the flexure arms on each side of the platform (Fig. 13), flexure arms with unequal lengths (defined by the hole locations in the 430 stainless steel strip), or tolerance between the clearance holes in the steel strip and screws used to attach the strip to the platform.

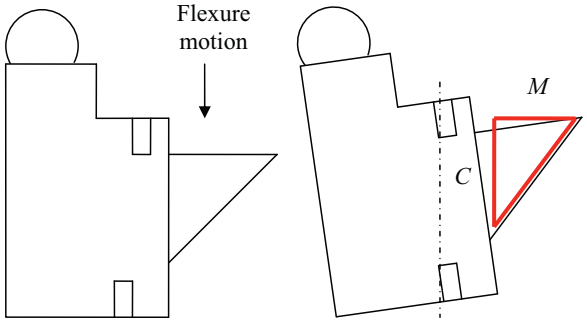

Fig. 13. Hole location error.

Fig. 14. Artifact dimensions.

4.2.3. Shaft/LVDT misalignments

If the shaft axis is not perpendicular to the flexure motion, a cosine error will be introduced. This angular misalignment could occur due to the fit between the shaft and linear bearings, the alignment between the bearings and bearing housing, and/or the alignment between the housing and tube. Again, the misalignment would have to be 8.5° in order for it to be the single error source. Finally, if the LVDT and shaft axes were misaligned, a similar cosine error would be introduced.

To determine whether the 0.989 *M* to *C* ratio could be attributed to this collection of assembly and setup misalignments, values were selected for each and the corresponding ratios were multiplied to see the combined effect. A value of ±0.5° for any of the cosine errors yields a ratio of 0.9999. For a ±0.05° tolerance on the 45° surface, the corresponding tangent error ratio is 0.998. The hole tolerances give a tangent error ratio of 0.994. The difference between the screw diameter and the clearance hole diameter is 0.1 mm. Given the distance between the holes and assuming a worst case scenario, a rotation of the platform by 0.36° could result which would give a tangent error ratio of 0.987. Multiplying these ratios gives a value of 0.979, which is lower than the experimental result. This suggests that the discrepancy between commanded and measured displacements could reasonably be attributed to these alignment errors. Naturally, a majority of these alignment errors could be eliminated by a monolithic flexure design machined from a single block of material.

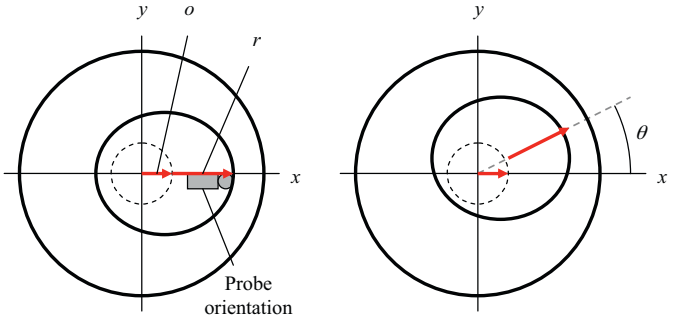

Fig. 15. Geometry of concentricity measurement.

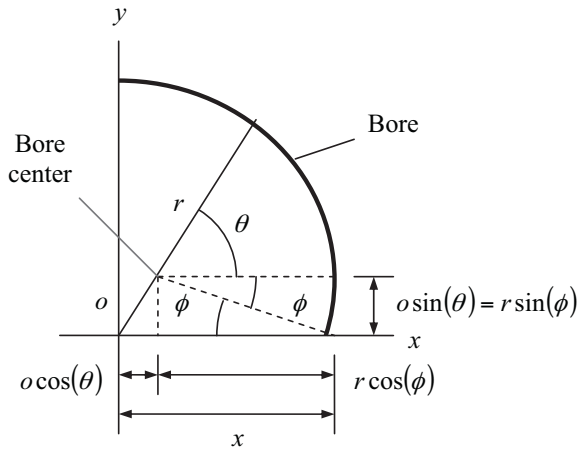

Fig. 16. Relationship between bore center offset, radius, and probe displacement measurement.

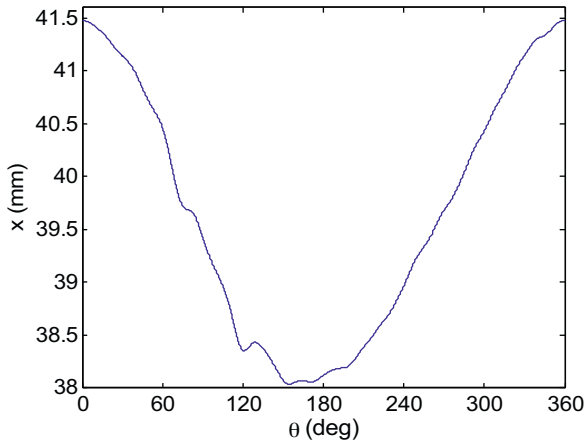

Fig. 17. Concentricity probe output, *x*, as a function of the part angular orientation.

5. Measurement procedures

5.1. Length probe

Based on the benchtop tests, it was determined that: (1) the length probe had sufficient accuracy to perform the desired measurement; and (2) for bias reduction, a calibration constant defined *in situ* could be applied to compensate for misalignments. The setup and measurement procedures for the length probe are outlined next.

Once the probe was mounted in the boring bar holder on turret A, the first step was to verify proper grounding and an accept-

Table 1
Artifact measurement results.

	CMM result (mm)	Probe result (mm)	Difference (mm)
L	316.662	316.684	−0.022
r	77.222	77.262	−0.040
o	0.014	0.006	0.008

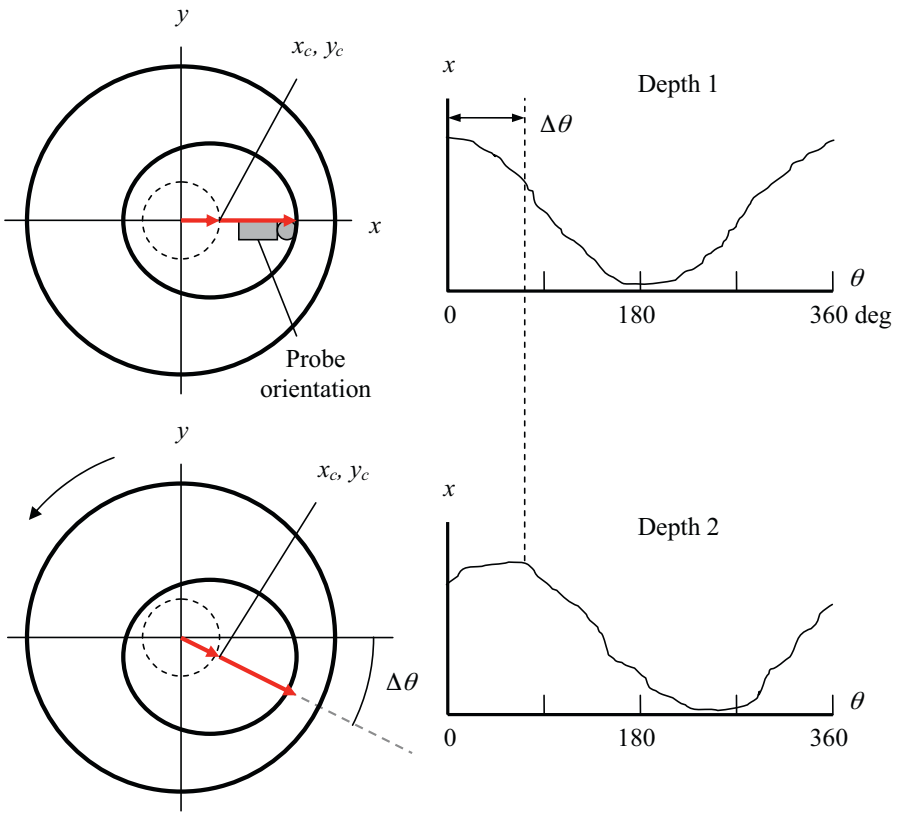

Fig. 18. Phase shift used to determine bore center location at different axial depths.

Table 2
Concentricity probe repeatability results.

Distance from front (mm)	Measurement number	Center offset (mm)	Radius (mm)	x_c (mm)	y_c (mm)
	1	0.175	39.825	0.175	0.000
	2	0.176	39.825	0.176	−0.002
6.35	3	0.177	39.827	0.177	−0.004
	4	0.177	39.827	0.177	−0.002
	5	0.177	39.827	0.177	−0.006
	Mean	0.176	39.826	0.176	−0.003
	Range	0.002	0.003	0.002	0.006
	1	0.289	40.114	0.289	0.000
	2	0.289	40.114	0.289	0.000
63.5	3	0.290	40.114	0.290	0.006
	4	0.290	40.117	0.290	0.000
	5	0.291	40.117	0.291	0.014
	Mean	0.290	40.115	0.290	0.004
	Range	0.001	0.003	0.001	0.014
	1	0.286	39.731	0.286	0.000
	2	0.286	39.733	0.286	0.012
127	3	0.287	39.733	0.286	−0.021
	4	0.287	39.736	0.286	−0.020
	5	0.287	39.736	0.287	−0.019
	Mean	0.287	39.734	0.286	−0.010
	Range	0.002	0.005	0.001	0.034
	1	0.324	39.627	0.324	0.000
	2	0.323	39.627	0.323	−0.005
190.5	3	0.324	39.627	0.324	−0.007
	4	0.324	39.627	0.324	0.000
	5	0.324	39.627	0.324	−0.005
	Mean	0.324	39.627	0.324	−0.004
	Range	0.000	0.000	0.000	0.007

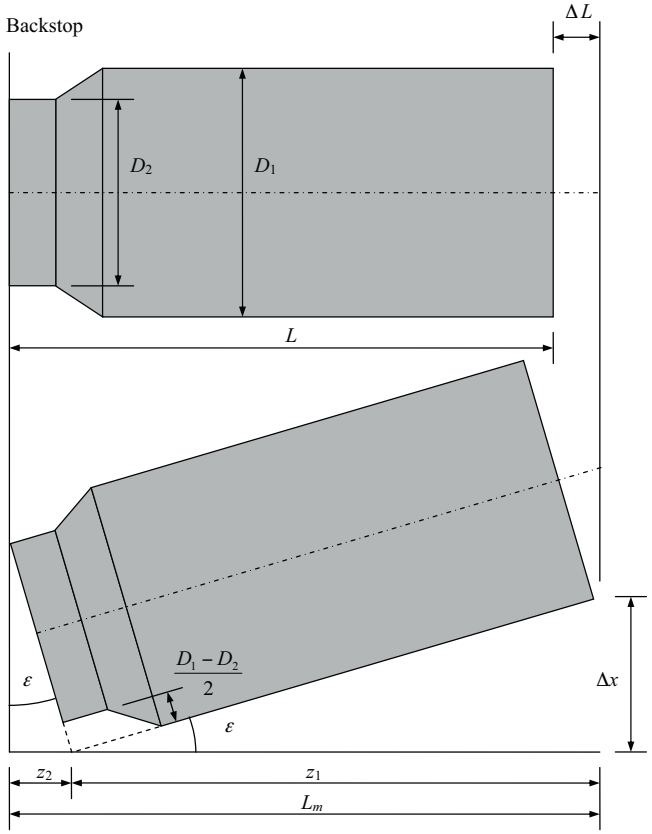

Fig. 19. Geometry for evaluating clamping effects on length measurement.

able noise level by analyzing voltage samples. Given an acceptable result, turret A was then used to position the probe against the part backstop (with the LVDT near its center of travel) located inside the chuck; the backstop provides a hard stop for inserting extrusions in the spindle collet chuck. To identify the *in situ* calibration constant, the turret was moved in z steps of 0.5 mm toward the backstop up to 7 mm and then back to the original location; the voltage was recorded at each location. The calibration constant, K_L, was set equal to the slope of the best fit line to the LVDT voltage versus z displacement data. The turret's z coordinate was then recorded as z_{ref} and the corresponding LVDT mean voltage was recorded as V_{ref}.

The presence of the part backstop provided a convenient reference surface for transforming the LVDT displacements into part dimensions with values larger than the LVDT range. The approach was to use the machine position (as reported by the controller) for macro-scale motion between the backstop and the unclamped end of the part. By combining the change in the z axis value with the difference in LVDT voltages when touching the backstop and part face, the length could be determined.

Once the reference location was identified, a part was chucked in the lathe and the probe was placed in contact (at approximately the LVDT's center of travel) with the part face. This turret z location was recorded as z_{meas} and, from this point forward in the measurement sequence, the machine's z value was not changed. Next, turret A was moved in the x direction until the probe was near the part's outer diameter. This marked the starting point for determining the location on the face with the highest bulge. Ten measurements were completed at equally spaced x locations from the outer diameter to the inner diameter. Since the voltage decreased as the LVDT pin was depressed, the machine x value associated with the lowest voltage identified the location where the bulge was largest (for this radial location). The turret x value was recorded as x_{peak} for this position.

Table 3
Length probe measurement results for 12 parts.

Part	Length (mm)
1	521.609
2	520.316
3	521.800
4	521.068
5	523.743
6	523.921
7	521.528
8	520.639
9	523.029
10	522.930
11	521.035
12	523.464
Mean	522.090
Range	3.604

The next step was a continuous measurement around the face of the part at the x_{peak} radial location. The part was rotated at approximately 18 rpm while the voltage was recorded at 5 kHz for 15 s (to capture multiple revolutions). After applying a Butterworth low pass filter with a 5 Hz cutoff frequency and isolating a single revolution of data, the lowest voltage, V_{meas}, was used to calculate the part's maximum length. See Eq. (1).

$$L = (z_{meas} - z_{ref}) - \left(\frac{V_{meas} - V_{ref}}{K_L}\right) \quad (1)$$

5.2. Concentricity probe

A similar process was used for the concentricity probe. However, because a diametric reference surface was not available on the lathe, an artifact was used to determine the probe's calibration constant and reference values. After installation in the boring bar holder, the noise floor for the probe was first verified. Next, the artifact (see Fig. 14) was chucked in the spindle and the spindle was locked to prevent motion of the artifact.[3] The turret was then positioned such that: (1) the probe was located inside the artifact; (2) the contact ball touched the larger inside diameter nearest the free end of the artifact; and (3) the flexure was deflected by half its total amount. To identify the calibration constant, K_C, the turret was moved in the x direction in steps of 1 mm up to 4 mm and then back to the original position; the mean voltage was recorded at each location. Next, the turret's z coordinate was recorded as z_{ref}. The spindle was then unlocked and the LVDT mean voltage from a single revolution of data collected during artifact rotation at 18 rpm for 15 s was recorded as V_{ref}.

Part measurements were completed by placing the probe in contact with the inner bore diameter at the desired depth (recall that the bore concentricity is a function of z location on the part). The x_{meas} axis location was recorded and then data was collected during rotation of the part, filtered, and one revolution was isolated as described previously. For subsequent measurement at other depths, the spindle was returned to the same orientation before beginning data collection.

The LVDT voltage recorded during part rotation provided information about both the hole radius and the offset of its center from the spindle axis, which was assumed to coincide with the part's axis of rotation defined by its outer diameter. Fig. 15 shows an exaggerated representation of the measurement as the part rotates counterclockwise. The outer circle represents the part's outer diameter, while the smaller solid circle represents the off-center bore.

[3] The artifact was measured using a touch-trigger probe coordinate measuring machine with an uncertainty of 12 μm over its work volume.

Table 4
Concentricity probe measurement results for 12 parts.

Part	Distance from front (mm)	Center offset (mm)	Radius (mm)	x_c (mm)	y_c (mm)
1	6.35	1.317	39.812	1.317	0.000
	63.5	0.917	40.218	0.908	−0.125
	127	0.878	39.870	0.793	−0.375
	190.5	0.965	39.863	0.864	−0.430
2	6.35	1.306	39.858	1.306	0.000
	82.55	0.474	39.949	0.335	0.335
	95.38	0.497	39.787	0.201	0.455
	184.15	0.471	39.517	−0.471	0.016
3	6.35	1.337	39.837	1.337	0.000
	63.5	0.923	40.069	0.918	0.095
	127	0.766	39.832	0.694	−0.322
	190.5	0.706	39.835	0.489	−0.509
4	6.35	1.439	40.063	1.439	0.000
	63.5	1.381	40.132	1.152	−0.762
	127	1.341	39.776	1.309	−0.291
	190.5	1.373	39.870	1.360	0.190
5	6.35	2.751	39.815	2.751	0.000
	63.5	2.301	40.063	2.300	0.060
	127	1.947	39.710	1.947	0.004
	214.35	1.721	39.756	1.714	−0.148
6	6.35	1.904	39.743	1.904	0.000
	63.5	1.588	40.071	1.587	−0.045
	127	1.350	39.921	1.305	−0.344
	190.5	1.130	39.868	1.074	−0.351
7	6.35	1.467	39.901	1.467	0.000
	63.5	1.474	40.107	1.474	−0.039
	127	1.372	39.817	1.365	−0.135
	190.5	1.350	39.837	1.325	0.258
8	6.35	2.286	39.995	2.286	0.000
	63.5	1.441	40.013	1.385	−0.396
	127	1.012	39.812	0.957	−0.329
	162.09	0.776	39.748	0.741	−0.231
9	6.35	1.913	40.056	1.913	0.000
	63.5	0.789	40.119	0.696	0.372
	127	0.234	39.715	0.220	0.078
	190.5	0.548	39.766	−0.546	0.049
10	6.35	1.359	39.756	1.359	0.000
	63.5	0.911	39.926	0.798	0.439
	127	0.946	39.505	0.873	0.363
	190.5	0.643	39.517	0.582	0.274
11	6.35	0.920	39.705	0.920	0.000
	63.5	0.717	40.063	0.604	0.386
	127	0.640	39.726	0.637	0.058
	190.5	0.596	39.530	0.590	−0.089
12	6.35	1.571	40.094	1.571	0.000
	63.5	0.882	40.107	0.847	−0.248
	127	0.735	39.647	0.429	−0.597
	190.5	0.591	39.632	−0.272	−0.525
Mean		1.166	39.861	1.057	−0.060
Range		2.517	0.714	3.297	1.217

As the part rotates, the bore center traces the smaller dashed circle. The center offset, o, is the distance from the spindle axis to the bore center. The bore radius, r, is the perpendicular distance from the bore center to the surface of the inner diameter. Note, however, that the probe measures x displacement only. Fig. 16 and Eq. (2) show how x relates to the radius and center offset.

$$x = o\cos(\theta) + r\cos(\phi) = o\cos(\theta) + r\cos\left(\sin^{-1}\left(\frac{o\sin(\theta)}{r}\right)\right) \quad (2)$$

Table 5
Selection of part programs to cover ranges in part length and bore diameter.

		Bore diameter		
		Small	Medium	Large
Length	Small	Part program 1	4	7
	Medium	2	5	8
	Large	3	6	9

To determine x, the location of the bore surface as a function of the spindle rotation angle, from the sinusoidal measured voltage, Eq. (3) is applied, where D is the reference diameter for the artifact. This equation is similar to Eq. (1), except that the artifact diameter is required because the reference voltage was not taken at a zero part reference location, but rather at a distance $D/2$ from the spindle axis of rotation. Additionally, the sign change was necessary because an increase in diameter caused an increase in voltage, while an increase in part length corresponded to a decrease in voltage. Finally, the difference between x_{meas} and x_{ref} must be divided by two because the controller gives x values in diametral coordinates.

$$x = \frac{x_{meas} - x_{ref}}{2} + \frac{V_{meas} - V_{ref}}{K_C} + \frac{D}{2} \quad (3)$$

Fig. 17 shows the filtered output, x, of the sensor as a function of angle of rotation, θ, for a single revolution of the part. This data was used to calculate both the radius and bore center offset from the spindle axis at the selected z location along the bore. The radius is the mean value and the offset is the difference between the max-

imum and minimum values divided by two. The variation in the bore center location is determined by comparing the results from different z locations; see Fig. 18. The phase shift for the maximum x was used in conjunction with Eqs. (4) and (5) to determine the coordinates of the bore center location, x_c and y_c, for the selected z depth inside the bore. Note that this approach requires that the starting spindle orientation is unchanged from one measurement to the next.

$$x_c = o\ \cos(\Delta\theta) \tag{4}$$

$$y_c = o\ \sin(\Delta\theta) \tag{5}$$

6. Measurement results

6.1. Artifact

The artifact shown in Fig. 14 was used to verify the probe's performance. Measurements of the artifact using the length and concentricity probes are compared to dimensions obtained using the CMM in Table 1. The probe values show reasonable agreement with CMM results. Although the disagreement is larger than the two-standard deviation uncertainty in the CMM measurements ($2 \times 0.012 = 0.024$ mm) for the radius measurement, the results are acceptable for this application. Note that the length probe algorithm identifies the maximum length of the part. For any chucking error (i.e., if the part axis is not parallel to spindle axis after clamping), the length probe measurement will therefore give a result which is larger than the actual part length. Chucking error is demonstrated for the part measurements in Section 6.2.

6.2. Extrusions

Repeated length measurements were performed on a single part (without removing it from the spindle) in order to establish the length probe measurement repeatability. After determining the calibration factor and locating the backstop, five length measurements were completed following the procedure described in Section 5.1. The resulting lengths were {521.272, 521.269, 521.266, 521.266, and 521.264} mm. The range is 0.008 mm with a standard deviation is 0.003 mm.

Similarly, repeated measurements were completed using the concentricity probe following the measurement procedure detailed in Section 5.2. A single part was measured five times each at four axial locations without unclamping the spindle chuck. The results are provided in Table 2. The range of variation for the center offset and radius was 0.005 mm or less for all five locations. The center location was less repeatable, but this is to be expected since the spindle angular orientation could not be reset to the same starting point between measurements (no spindle encoder access was available). To approximately reorient the part after each test, a mark was scribed on the part and matched to a corresponding mark on the spindle housing.

To evaluate the influence of chucking repeatability, the same part used for the length measurements was removed from the spindle and then reclamped. The new length (i.e., the point on the part face that gave the largest extension beyond the backstop) was 521.035 mm. This result is 0.232 mm less than the mean value of the five measurements obtained without unclamping the part (521.267 mm). For a second part, the process was repeated and the difference was 0.216 mm. These differences are larger than the length probe measurement accuracy and suggest non-repeatability in the part clamped condition. To verify the clamping inconsistency, a dial indicator was used to measure the radial error motion at the part surface for multiple unclamp-remove-replace-clamp cycles using a single part. Deviations ranged from ±0.61 mm to ±2.2 mm.

To explore the effect of chucking variation on the measured length, the geometry shown in Fig. 19 can be used. Each time a part is chucked, there is potential for a ΔL change in length (equal to the difference between L_m and L in Fig. 19). To calculate ΔL for a given radial error motion, $\pm\Delta x$, the angle ε is first calculated using Eq. (6). Next, the axial dimensions z_1 and z_2 are computed using Eqs. (7) and (8). The measured length, L_m, is then taken to be the sum of z_1 and z_2 and, finally, ΔL is calculated. For $L = 520.7$ mm, $\Delta x = 0.61$ mm, $D_1 = 174.6$ mm, and $D_2 = 136.5$ mm, ΔL is 0.182 mm. If $\Delta x = 2.2$ mm, the corresponding ΔL is 0.653 mm. This range encompasses the variation in on-machine length measurements and verifies that clamping non-repeatability is a significant contributor to part length deviation.

$$\varepsilon = \sin^{-1}\left(\frac{\Delta x}{L}\right) \tag{6}$$

$$z_1 = \frac{\Delta x}{\tan(\varepsilon)} \tag{7}$$

$$z_2 = \sin(\varepsilon)\left(\frac{D_1 - D_2}{2} + D_2\right) \tag{8}$$

Next, 12 different parts were measured sequentially. The length measurement results are shown in Table 3. The range was 3.604 mm with a mean of 522.090 mm. Two lengths (parts 2 and 8) were outside the expected range of 520.7 mm +6.4/−0 mm.

The concentricity probe was also used to measure the 12 parts. As shown in Fig. 3, the nominal bore radius was 40.75 mm with a tolerance of +0/−0.635 mm. Table 4 displays the results for measurements taken at axial locations of {6.35, 63.5, 127, and 190.5} mm from the free end of the part. Some measurements deviated from these locations to avoid significant surface deformations (pits or protrusions) within the bore, e.g., see part 2. Only three radius measurements were within the specified tolerance. All other values were smaller by an average of 0.271 mm.

7. Conclusions

In this study, two contact probes were designed, fabricated, and implemented to measure the length and bore concentricity of cylindrical, extruded tool joints while clamped in a production lathe spindle. The length probe consisted of an LVDT, a spring-preloaded shaft supported by linear bearings used to isolate the LVDT from side loads, and a hardened steel sphere to contact the rough surface of the parts. The concentricity probe incorporated a parallelogram leaf-type flexure and 45° surface to transfer radial deviations to the LVDT axis. In both cases, the LVDT output was used in conjunction with to the lathe turret position to determine the extruded part dimensions prior to machining. Measurements were completed on 12 parts and results for length, internal diameter, and bore concentricity were presented.

Given the pre-machining part dimensions, a selection could be made from a pre-defined matrix of part programs that are defined using the anticipated range of part dimensions. The part program would be selected such that depths of cut that are significantly larger than expected (based on nominal part dimensions) would be avoided. See Table 5 as an example. In this way, the time-consuming approach of defining the part program based on the largest possible part would be replaced and the cycle time and machining cost would be reduced while increasing the tool life.

Acknowledgement

The authors gratefully acknowledge financial support from General Dynamics-OTC, St. Petersburg, FL (Dr. D. Bartles, program manager).

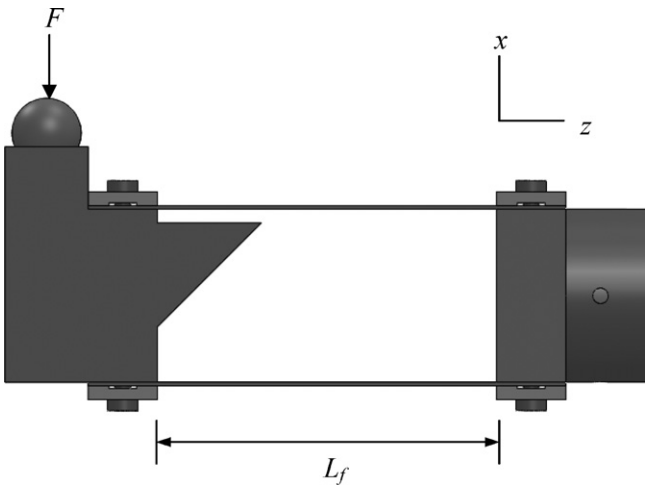

Fig. A1. Flexure dimensions.

Appendix A.

The parallelogram leaf-type flexure design is shown in Fig. A1, where the contact force, F, imposed by the bore surface and the length, L_f, of the parallel 430 stainless steel flexure arms are identified. Because the platform does not follow a perfectly linear motion profile in the x direction, parasitic motion in the z direction must also be considered. Eq. (A1) can be used to approximate the z parasitic motion for an x direction platform motion, δ [5]. The deflected flexure is shown in Fig. A2. For a flexure length of $L_f = 62.2$ mm and a deflection of $\delta = 5$ mm, the corresponding parasitic motion is 0.24 mm.

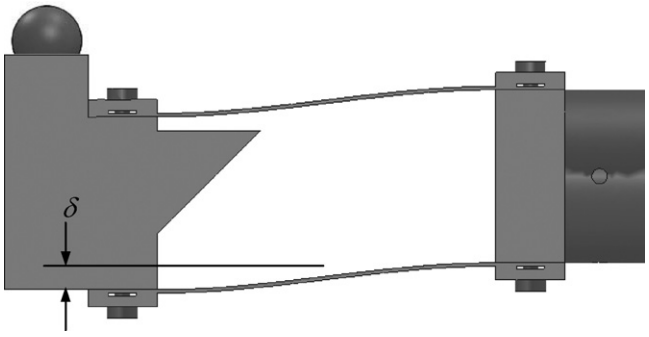

Fig. A2. Deflected flexure.

$$z = \frac{3\delta^2}{5L_f} \tag{A1}$$

References

[1] Yandayan T, Burdekin M. In-process dimensional measurement and control of workpiece accuracy. International Journal of Machine Tools and Manufacture 1997;37:1423–39.
[2] Vacharanukul K, Mekid S. In-process dimensional inspection sensors. Measurement 2005;38(3):204–18.
[3] efunda, LVDT: Theory, http://www.efunda.com/designstandards/sensors/lvdt/lvdt_theory.cfm [accessed 2/21/2010].
[4] RDP Electrosense, DCTH Series DC to DC LVDT Displacement Transducer, http://www.rdpe.com/us/dcth.htm [accessed 2/21/2010].
[5] Smith ST. Flexures: Elements of Elastic Mechanisms. Boca Raton, FL: CRC Press LLC; 2000.